BIOCHEMISTRY
including biophysical chemistry & molecular biology

Article

pubs.acs.org/biochemistry

Crystal Structure and Characterization of Particulate Methane Monooxygenase from *Methylocystis* species Strain M

Stephen M. Smith,[†] Swati Rawat,[‡] Joshua Telser,[†,§] Brian M. Hoffman,[†] Timothy L. Stemmler,*[,‡] and Amy C. Rosenzweig*[,†]

[†]Departments of Molecular Biosciences and of Chemistry, Northwestern University, Evanston, Illinois 60208, United States

[‡]Department of Biochemistry and Molecular Biology, Wayne State University, School of Medicine, Detroit, Michigan 48201, United States

Supporting Information

ABSTRACT: Particulate methane monooxygenase (pMMO) is an integral membrane metalloenzyme that oxidizes methane to methanol in methanotrophic bacteria. Previous biochemical and structural studies of pMMO have focused on preparations from *Methylococcus capsulatus* (Bath) and *Methylosinus trichosporium* OB3b. A pMMO from a third organism, *Methylocystis* species strain M, has been isolated and characterized. Both membrane-bound and solubilized *Methylocystis* sp. strain M pMMO contain ~2 copper ions per 100 kDa protomer and exhibit copper-dependent propylene epoxidation activity. Spectroscopic data indicate that *Methylocystis* sp. strain M pMMO contains a mixture of Cu^{I} and Cu^{II}, of which the latter exhibits two distinct type 2 Cu^{II} electron paramagnetic resonance (EPR) signals. Extended X-ray absorption fine structure (EXAFS) data are best fit with a mixture of Cu−O/N and Cu−Cu ligand environments with a Cu−Cu interaction at 2.52−2.64 Å. The crystal structure of *Methylocystis* sp. strain M pMMO was determined to 2.68 Å resolution and is the best quality pMMO structure obtained to date. It provides a revised model for the pmoA and pmoC subunits and has led to an improved model of *M. capsulatus* (Bath) pMMO. In these new structures, the intramembrane zinc/copper binding site has a different coordination environment from that in previous models.

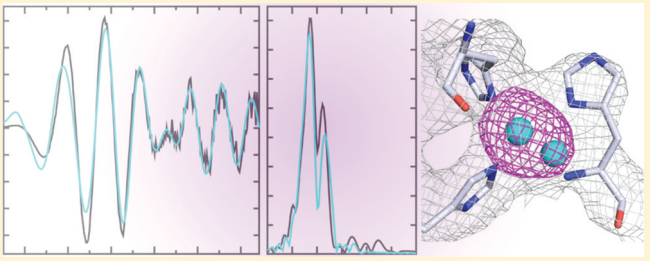

Methanotrophic bacteria are obligate C1 metabolizers that utilize methane as a carbon and energy source.[1] The initial step in their metabolic pathway, the oxidation of methane to methanol, is catalyzed by two different methane monooxygenase (MMO) enzymes. Most methanotrophs produce a membrane-bound enzyme called particulate MMO (pMMO), and some can also produce a soluble, cytoplasmic enzyme (sMMO) under conditions of copper starvation.[2] Although both MMOs can break the strong C−H bond in methane (104 kcal/mol), their overall structures are completely different. sMMO is an $\alpha_2\beta_2\gamma_2$ dimer with a single metal binding site, a carboxylate-bridged diiron center responsible for methane oxidation.[3] Much is known about O_2 activation at the diiron center, O_2 and substrate/product access to the active site, and activity modulation by other protein components.[4,5] In contrast to sMMO, the chemistry of methane oxidation by pMMO is not well understood.

Crystal structures of *Methylococcus capsulatus* (Bath)[6,7] and *Methylosinus trichosporium* OB3b[8] pMMOs to 2.8 and 3.9 Å resolutions, respectively, reveal an $\alpha_3\beta_3\gamma_3$ trimer composed of the pmoB, pmoA, and pmoC polypeptides and multiple metal binding sites. In both pMMO structures, the periplasmic regions of the pmoB subunit house a copper binding site modeled as a dicopper center on the basis of extended X-ray absorption fine structure (EXAFS) data[9,10] and the *M. capsulatus* (Bath) pMMO crystallographic data.[6] A second copper site, modeled as a monocopper center, is also present in the *M. capsulatus* (Bath) pmoB subunit. A metal binding site within the membrane-spanning pmoC and pmoA subunits is occupied by zinc in *M. capsulatus* (Bath) pMMO[6] and copper in *M. trichosporium* OB3b pMMO.[8] On the basis of activity data and characterization of recombinant pmoB fragments, we have proposed that the dicopper center in pmoB is the active site of pMMO.[11]

Other researchers have proposed that the pMMO active site is a diiron center located at the crystallographically observed transmembrane zinc/copper site[12,13] or a tricopper center housed within a transmembrane hydrophilic patch of residues.[14] The latter model includes the binding of 10 additional copper ions to the soluble C-terminus of pmoB.[15] The differing views of the active site derive from variations in the metal content and spectroscopic properties of pMMO samples isolated by different laboratories. Most studies have focused on pMMO from *M. capsulatus* (Bath) and *M. trichosporium* OB3b.[2,13,16] Purified *M. capsulatus* (Bath) pMMO has been reported to contain 2−20 Cu and 0−2 Fe

Received: May 23, 2011
Revised: October 19, 2011
Published: October 20, 2011

per 100 kDa $\alpha\beta\gamma$ protomer,[10,17−20] whereas purified *M. trichosporium* OB3b pMMO contains 2 Cu per protomer with only trace amounts of Fe.[8,21] Electron paramagnetic resonance (EPR) spectra of both pMMOs indicate the presence of type 2 Cu^{II},[2,16] but the relationship between these EPR signals and the crystallographically detected copper centers remains unclear. Chan and co-workers also observe an isotropic signal at $g \sim 2.1$, which they interpret as a ferromagnetically coupled trinuclear Cu^{II} cluster.[22] X-ray absorption spectroscopic (XAS) studies indicate that as-isolated purified pMMO contains a mixture of Cu^{I} and Cu^{II} and a Cu-containing cluster with a short Cu−Cu distance of ∼2.5 Å,[8−10] which is correlated with the presence of the crystallographic dicopper center and with methane oxidation activity.[11]

To obtain additional data regarding the structure and metal centers of pMMO, we have isolated and characterized pMMO from a third organism, the type II methanotroph *Methylocystis* species strain M. The pmoB, pmoA, and pmoC subunits from this organism are 82%, 87%, and 88% identical to the corresponding subunits from *M. trichosporium* OB3b, also a type II methanotroph, and 47%, 58%, and 62% identical to the corresponding subunits from *M. capsulatus* (Bath), a type X methanotroph. The metal content, activity, and spectroscopic properties of *Methylocystis* sp. strain M pMMO are consistent with what we have observed for the other two pMMOs. Importantly, *Methylocystis* sp. strain M pMMO crystallizes more reproducibly than *M. capsulatus* (Bath) pMMO, and the crystals diffract to higher resolution than those of both the *M. capsulatus* (Bath) and *M. trichosporium* OB3b pMMOs. The *Methylocystis* sp. strain M pMMO structure, determined to 2.68 Å resolution, is higher quality than the previously reported structures[6,8] and provides a revised model for the pmoA and pmoC subunits. The new model has implications for the crystallographic zinc/copper site and has led to an improved structure of *M. capsulatus* (Bath) pMMO.

MATERIALS AND METHODS

Bacterial Growth. Cultures of *Methylocystis* sp. strain M were grown at 30 °C using a nitrate mineral salts medium (0.85 g/L $NaNO_3$, 0.17 g/L K_2SO_4, 0.04 g/L $MgSO_4{\cdot}7H_2O$, 0.01 g/L $CaCl_2{\cdot}2H_2O$) supplemented with a trace element solution (0.29 mg/L $ZnSO_4{\cdot}7H_2O$, 0.17 mg/L $MnCl_2{\cdot}6H_2O$, 0.06 mg/L H_3BO_3, 0.05 mg/L $Na_2MoO_4{\cdot}2H_2O$, 0.05 mg/L $CoCl_2{\cdot}6H_2O$, 0.08 mg/L KI, 0.13 mg/L $CuSO_4{\cdot}5H_2O$), 50 μM $CuSO_4{\cdot}5H_2O$, and 40 μM $FeSO_4{\cdot}7H_2O$. Fermentations (12 L) were initiated using 5−10 g of resuspended cell stocks directly or from single colonies grown on agar plates (supplemented with 10 μM $CuSO_4{\cdot}5H_2O$) that were serially increased to 1 L (1 mL, 5 mL, 50 mL, etc.) before inoculation into 11 L of media. A 3:1 ratio of air to methane was maintained during growth with a constant agitation rate of 300 rpm. The pH was maintained between 7.0 and 7.3 using a 100 mM phosphate buffer with fine adjustments made during the growth using 2 M H_2SO_4 and 1 M NaOH. Cells were harvested at an OD_{600} of 5−6 and centrifuged at 8000*g* for 10 min. Pelleted cells were resuspended and washed in 25 mM PIPES, pH 7.0, centrifuged, flash frozen in liquid nitrogen, and stored at −80 °C.

Membrane Isolation and pMMO Solubilization. Frozen cells were resuspended in lysis buffer (25 mM PIPES, pH 7.3, 500 mM NaCl, 1 mM benzamidine) and either sonicated on ice for 10 min with 1 s on/off pulses or passed three times though a microfluidizer with the heat exchanging coil submerged in an ice−water bath at a constant pressure of 180 psi. Cell debris was removed by centrifugation at 22000*g* for 2 h. Intracytoplasmic membranes were pelleted using ultracentrifugation at 160000*g* for 2 h. These crude pMMO membrane isolations were washed by resuspending and homogenizing in fresh lysis buffer, followed by ultracentrifugation for an additional 2 h. Homogenized crude pMMO membranes diluted to 10−20 mg/mL were either used immediately or flash frozen in liquid nitrogen and stored at −80 °C. Membranes treated with CN^- were prepared as described previously.[11,23] pMMO was solubilized by adding 1.2 mg of *n*-dodecyl-β-D-maltopyranoside (DDM) per mg of protein as determined by the Bio-Rad *DC* protein assay. The solution was stirred at 4 °C for 15 min and ultracentrifuged for 30 min to remove insoluble material and excess lipids. This solubilization procedure results in approximately 90−95% pure pMMO with no further purification necessary (Figure 1). Attempts to further purify pMMO by size exclusion or anion exchange chromatography resulted in subunit degradation.

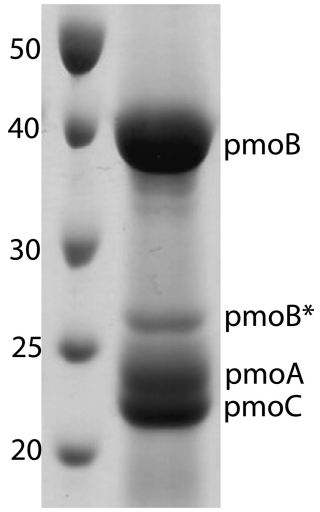

Figure 1. SDS-PAGE gel of solubilized *Methylocystis* sp. strain M pMMO. Molecular mass standards are labeled in kDa. The band labeled pmoB* corresponds to a proteolytic fragment of pmoB with an N-terminus starting at residue Gln 260.

Metal Analysis and Activity Assays. A Varian Vista-MPX CCD Simultaneous ICP-OES instrument was used to determine the metal ion content of crude pMMO membranes and solubilized pMMO. Samples were digested in 5% trace metal grade nitric acid, and standard curves were generated using dilutions of copper, zinc, and iron atomic absorption standards (Sigma-Aldrich). All samples were measured in triplicate from at least two independent isolations. Activity was determined by the propylene epoxidation assay using duroquinol as a reductant as described[11,23] with minor modifications. In brief, 200 μL of pMMO (10−20 mg/mL) was incubated with saturating amounts of freshly prepared duroquinol and 2 mL of propylene in a septum sealed vial and shaken at 200 rpm for 3 min in a 37 °C water bath. The amount of propylene oxide produced was detected by gas chromatography using either a Hewlett-Packard 5890A GC or an Agilent Technologies 7890A GC equipped with a Porapak Q column (Supelco) and quantitated using a standard curve generated with pure propylene oxide (Sigma-Aldrich). All samples were measured in duplicate from at least two independent isolations. For CN^- treated samples, metal

Table 1. Metal Content and Activity of *Methylocystis* sp. strain M pMMO[a]

sample	Cu per 100 kDa pMMO	Fe per 100 kDa pMMO	Zn per 100 kDa pMMO	activity (nmol propylene oxide/(min mg))
membrane-bound	2.29 ± 0.22	0.59 ± 0.09	0.10 ± 0.02	5.3 ± 1.4
CN^- treated	0.05 ± 0.01	0.29 ± 0.11	ND	0
CN^- treated + 2Cu				1.34 ± 0.06
solubilized	2.11 ± 0.46	0.43 ± 0.02	0.06 ± 0.02	1.24 ± 0.21

[a]All samples were measured in triplicate and are the average of at least two independent isolations.

equivalents were added, mixed, and incubated at room temperature for 30 min prior to activity measurements.[23]

EPR Spectroscopy. Membrane-bound and solubilized pMMO samples were prepared as above with the addition of 10% glycerol (final concentration) to all the buffers. Reconstituted pMMO samples were incubated with copper equivalents for 30 min prior to glycerol addition. The reconstituted samples were prepared from the same protein batch as the activity assay samples in order to correlate the amount of EPR active copper with enzyme activity. All samples were measured on a modified Varian E-4 spectrometer at 77 K. Quantitation of EPR active Cu^{II} was performed by comparison with a standard curve generated from copper-EDTA solutions ($CuSO_4 \cdot 5H_2O$ in 1 mM EDTA, 0.5 M NaCl, 10% glycerol) of known concentrations. All samples were background and baseline corrected prior to quantitation by double integration. Spectra were simulated using a modified version of the program QPOWA.[24,25]

X-ray Absorption Spectroscopy. Samples of as-isolated, reduced, copper-reconstituted, and oxidized pMMO were prepared in 50 mM HEPES, pH 7.5, containing 0.03% *n*-undecyl-β-D-maltopyranoside (UDM) and contained 0.5−1.0 mM copper. All samples except for the copper-reconstituted sample were solubilized as described above. The copper-reconstituted sample was membrane-bound and was prepared by CN^- treatment as described previously.[11,23] XAS data were collected at the Stanford Synchrotron Radiation Laboratory (SSRL) on beamline 9-3 using a Si(220) double crystal monochromator equipped with a harmonic rejection mirror. Samples were maintained at 10 K using an Oxford Instruments continuous-flow liquid helium cryostat, and protein fluorescence excitation spectra were collected using a 30-element Ge solid-state array detector. A 0.6 μm wide nickel filter was placed between the cryostat and detector to filter scattering fluorescence not associated with protein Cu signals. XAS spectra were measured as detailed previously.[11] All data represent the average of 5−6 scans, and spectra were collected on at least two independent and reproducible samples. XAS data were processed with the Macintosh OS X version of the EXAFSPAK program suite[26] integrated with the Feff v7 software[27] for theoretical model generation. Data reduction and fitting analysis were performed according to published protocols (refs 9 and 11, Supporting Information) using single scattering Feff v7 theoretical models, calculated for carbon, oxygen, sulfur, and copper coordination to simulate copper-ligand environments, with values for the scale factors (Sc) and E_0 calibrated as described elsewhere.[9]

Crystallization and Structure Determination. Solubilized pMMO was concentrated to ∼250 μL using a 15 mL Amicon Ultra 50,000 MWCO filter and exchanged into crystallization buffer (50 mM HEPES, pH 7.5, 0.03% *n*-undecyl-β-D-maltopyranoside (UDM)) by diluting to ∼15 mL and concentrating back to 250 μL. The concentrated sample was then diluted to 10 mg/mL with crystallization buffer. Initial screening using the Qiagen Classics with 96-well sitting drop trays (50 μL well solution, 1 μL protein, and 1 μL well solution in drops) produced microcrystals in condition #79 (0.1 M MES, pH 6.5, 25% PEG 550 MME, 0.01 M $ZnSO_4$) at 22 °C. This condition was reproducible in 24-well sitting drop trays (750 μL well solution, 2 μL protein, and 2 μL well solution in drops) and formed small crystals that diffracted to ∼7 Å resolution. Screening different molecular weight PEG solutions together with the Hampton additive screen yielded crystals that diffracted to better than 5 Å resolution. Subsequent optimization resulted in a condition (0.1 M MES, pH 6.5, 18% PEG 750 MME, 0.03 M glycyl glycyl glycine, 0.01 M $ZnSO_4$) that reproducibly gave crystals diffracting to ∼3 Å resolution. The best of these crystals diffracted to better than 2.8 Å resolution and were produced in 1−2 weeks by mixing 2 μL of protein with 2 μL of crystallization buffer in sitting drops at 22 °C.

Crystallographic data collection was performed at the Advanced Photon Source (Argonne National Laboratory) using LS-CAT beamline 21-ID-D and GM/CA-CAT beamline 23-ID-D. The data were integrated and scaled using HKL2000.[28] The crystals belong to the space group $P2_12_12_1$ with unit cell dimensions of a = 107.7, b = 178.3, and c = 183.1 Å. A molecular replacement solution was obtained with PHASER[29] using the coordinates of *M. capsulatus* (Bath) pMMO (PDB code 1YEW) as a starting model. Multiple rounds of model building and refinement with COOT[30] and REFMAC5[31] were needed to fit the *Methylocystis* sp. strain M pMMO subunit sequences to the electron density. Tight noncrystallographic symmetry (NCS) was used throughout the refinement for pmoB residues 30−414, pmoA residues 35−223, and pmoC residues 26−179. The final model contains pmoB residues 29−414, pmoA residues 11−252, pmoC residues 16−197 and 225−252, two polyalanine helices comprising 16 and 19 residues, respectively, four copper ions, 9 zinc ions, and three water molecules. A Ramachandran plot calculated with MolProbity[32] indicates that 90.3% of residues are in the favored regions and 96.7% of residues are in the allowed regions. The final *Methylocystis* sp. strain M pMMO coordinates were then used as a molecular replacement model to solve and refine the *M. capsulatus* (Bath) pMMO structure using the original data.[6] The new refined model contains pmoB residues 33−414, pmoA residues 7−191 and 213−245, pmoC residues 45−224 and 254−286, 9 copper ions, and 9 zinc ions. A Ramachandran plot calculated with MolProbity[32] indicates that 89.5% of residues are in the favored regions and 97.7% of residues are in the allowed regions.

RESULTS AND DISCUSSION

Metal Content and Activity. Membrane-bound and solubilized pMMO from *Methylocystis* sp. strain M contain ∼2 Cu per 100 kDa protomer (Table 1). This is significantly less copper than that measured in membrane-bound preparations of *M. capsulatus* (Bath) pMMO (4−59 Cu/100 kDa

pMMO)[2,16] but similar to the amounts reported for *M. trichosporium* OB3b pMMO (4−5 Cu per 100 kDa membrane-bound pMMO and 1−2 Cu per 100 kDa purified pMMO).[8,21] Recent studies indicate that only 2−3 copper ions are required for *M. capsulatus* (Bath) pMMO activity, suggesting that some copper is bound adventitiously and/or associated with the copper chelator methanobactin.[11] Unlike pMMO from *M. trichosporium* OB3b,[8,21] the *Methylocystis* sp. strain M samples do contain measurable iron (0.59 ± 0.09 Fe/100 kDa pMMO for membrane-bound and 0.43 ± 0.02 Fe/100 kDa pMMO for solubilized) (Table 1). The optical spectrum of solubilized *Methylocystis* sp. strain M pMMO exhibits a peak at ∼412 nm, suggestive of heme contamination, which is commonly observed for *M. capsulatus* (Bath) pMMO[9,10] and may account for at least some of the measured iron. Negligible amounts of zinc are detected.

The specific activity of membrane-bound *Methylocystis* sp. strain M pMMO is 5.3 ± 1.4 nmol propylene oxide/(min mg) (average of 10 samples) (Table 1), which is comparable to the specific activity of 2−5 nmol propylene oxide/(min mg) reported for pMMO from *M. trichosporium* OB3b.[8,21,33] The addition of 1 equiv of $CuSO_4$ per 100 kDa pMMO prior to activity measurements typically increases the membrane-bound pMMO specific activity by ∼5−20%, suggesting that the copper active site is not fully loaded (vide infra). Further copper additions decrease activity. Solubilized *Methylocystis* sp. strain M pMMO has a specific activity of 1.24 ± 0.21 nmol propylene oxide/(min mg) (average of two samples), which is in the range of that reported for solubilized *M. trichosporium* OB3b pMMO.[8] Since membrane-bound and solubilized *M. trichosporium* OB3b pMMO contain less than 0.01 Fe/100 kDa pMMO,[8] it is unlikely that the iron in *Methylocystis* sp. strain M pMMO (Table 1) accounts for the observed enzyme activity. However, these data should be interpreted with the caveat that the activity levels for all isolated pMMO samples are typically 1−10% of that measured for whole cells.[13]

Cyanide treatment of *Methylocystis* sp. strain M membrane-bound pMMO removes ∼98% of the copper and ∼49% of the iron (Table 1) and abolishes all activity. Addition of 2 equiv of copper restores ∼25% of the as-isolated activity (1.34 ± 0.06 nmol propylene oxide/(min mg), average of two samples). Similar results were obtained upon treatment of *M. capsulatus* (Bath) pMMO with cyanide, with addition of 2−3 equiv of copper restoring ∼70% of activity.[11,23] Typically, adding more than 2 equiv of copper results in inhibition, which is attributed to hydrogen peroxide formation.[11,33] The difference in the level of activity restored by addition of copper to cyanide treated pMMO from *Methylocystis* sp. strain M and *M. capsulatus* (Bath) is consistent with the copper in *Methylocystis* sp. strain M pMMO being more labile. This increased lability may be related to the absence of the monocopper center in pmoB (ref 8; vide infra). While apparently not catalytically active, the presence of the monocopper site likely stabilizes the residues involved in copper binding at the dicopper site.[11]

EPR Spectroscopy. The X-band EPR spectra of membrane-bound and solubilized Methylocystis sp. strain M pMMO exhibit a typical type 2 Cu^{II} signal (Figure 2B,C). According to spin quantitation using a Cu^{II} standard, ∼69% of the copper in the membrane-bound sample and ∼43% of the copper in the solubilized sample are EPR active. A type 2 Cu^{II} signal has been observed in whole cell, membrane-bound, and purified pMMO samples from several different organisms.[8,10,17,18,34−36] There is no evidence for the signal attributed to a trinuclear copper cluster.[22,37,38] A simulation of the solubilized pMMO EPR spectrum indicates the presence of two type 2 Cu^{II} signals (Figure 2D). The major component, with parameters $g_\perp$ = 2.052, $g_\parallel$ = 2.247, $A(^{63}Cu)_\parallel$ = 570 MHz, and $A(^{63}Cu)_\perp$ = 60 MHz, is identical to the major component that constitutes at least 80% of the signal in the EPR spectrum of purified *M. trichosporium* OB3b pMMO.[8] The *M. trichosporium* OB3b pMMO minor component has g values $g_\perp$ = 2.060 and $g_\parallel$ = 2.225 and resolved hyperfine coupling of about 40 MHz to two equivalent ^{14}N nuclei.[8] By contrast, the second component of the *Methylocystis* sp. strain M pMMO EPR spectrum has parameters $g_\perp$ = 2.04 and $g_\parallel$ = 2.215, exhibits no observable ^{14}N hyperfine coupling, and is at least 70% of the intensity of the major component (an approximation due to uncertainty in the perpendicular region at this microwave frequency). For both *M. trichosporium* OB3b and *Methylocystis* sp. strain M pMMO, the

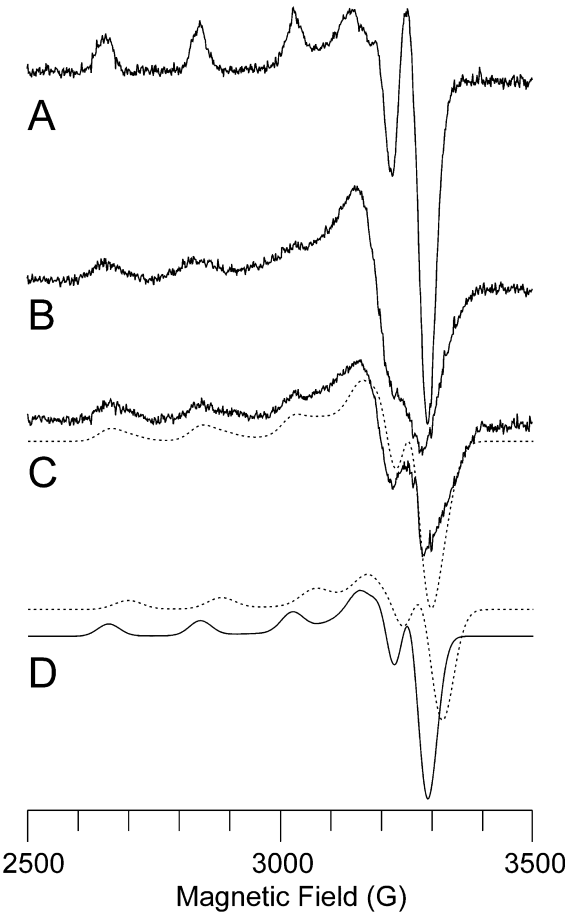

Figure 2. X-band EPR spectra of *Methylocystis* sp. strain M pMMO. (A) Cu-EDTA standard (250 μM). (B) Membrane-bound pMMO. (C) Solubilized pMMO with simulation (dashed line) generated by summing two contributing type 2 Cu^{II} centers. (D) Individual simulated spectra of the two components in (C). The experimental spectra are offset for clarity, but their intensities are meaningful since the spectra were recorded under identical conditions. Experimental parameters: microwave frequency, 9.21 GHz; microwave power, 15 dB; modulation amplitude, 5.000 G; receiver gain, 1.25 × 10^2; time constant, 0.3 s; temperature, 77 K; 2 min scan. Simulation parameters for major component (solid line in part D): relative integrated intensity, 1.0; $g_\perp$ = 2.052, $g_\parallel$ = 2.247, $A(^{63}Cu)_\parallel$ = 570 MHz, $A(^{63}Cu)_\perp$ = 60 MHz. Simulation parameters for minor component (dashed line in part D): relative integrated intensity, 0.7; $g_\perp$ = 2.04, $g_\parallel$ = 2.215, $A(^{63}Cu)_\parallel$ = 570 MHz, $A(^{63}Cu)_\perp$ = 60 MHz.

$A(^{63}Cu)_{\|}$ value for the major and minor components is indistinguishable.

The X-band EPR spectrum of cyanide-treated membrane-bound pMMO following addition of 2 equiv of copper is similar to that of as-isolated pMMO (Figure S1). Interestingly, quantitative comparisons to a Cu^{II} standard indicate that only ~50% of the total copper in these reconstituted samples is EPR-active. Assuming that these copper ions occupy the dicopper center, these data could be consistent with a previously suggested trapped valence $Cu^{I}Cu^{II}$ site.[39] Upon addition of a third equivalent of copper, ~67% of the total copper is EPR-active. Thus, the third copper is Cu^{II}, but it is not clear if or where it is binding. One possibility is that this third equivalent binds in the transmembrane site occupied by zinc in the *M. capsulatus* (Bath)[6] and *Methylocystis* sp. strain M (vide infra) pMMO crystal structures.

XAS Spectroscopy. The XANES spectrum of dithionite-reduced, solubilized *Methylocystis* sp. strain M pMMO (Figure 3A) closely resembles spectra reported for three to four-coordinate Cu^{I} compounds, based on the intensity of the 1s → 4p transition, the overall edge structure, and the lack of any discernible 1s → 3d feature.[40] The XANES spectrum for as-isolated, solubilized pMMO (Figure 3B) has a reduced, but observable, 1s → 4p transition and a weak 1s → 3d feature, consistent with copper in this sample being a mixture of Cu^{I} and Cu^{II} or a predominantly square or tetragonal Cu^{II} complex. The XANES spectrum of Cu-reconstituted, membrane-bound pMMO (Figure 3C) is nearly identical to that of as-isolated solubilized pMMO (Figure 3B). The oxidized pMMO sample treated with hydrogen peroxide has a XANES spectrum consistent with a square or tetragonal Cu^{II} coordination environment (Figure 3D).

Fourier transforms of the Cu EXAFS data for as-isolated, reduced, Cu-reconstituted, and oxidized pMMO all show two scattering interactions corresponding to nearest-neighbor ligands at approximately 2 and 2.5 Å (Figure 4 and Table 2).

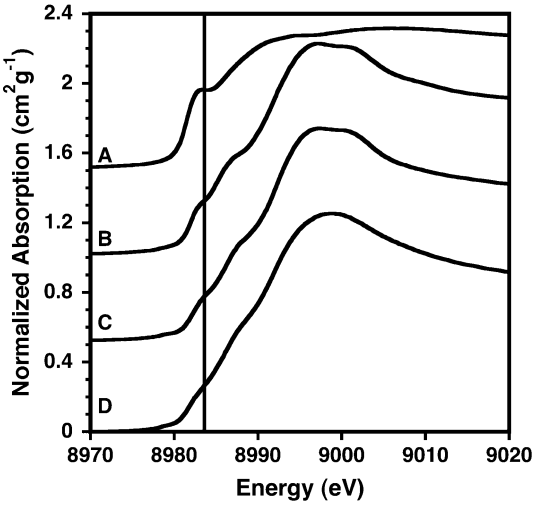

Figure 3. Copper XANES spectra of *Methylocystis* sp. strain M pMMO. The spectra for (A) reduced, (B) as-isolated, (C) Cu-reconstituted, membrane-bound, and (D) oxidized samples are shown. The reduced, as-isolated, and oxidized samples were solubilized. The dashed vertical line at ca. 8984 eV identifies spectral features corresponding to the Cu^{I} 1s → 4p transition. Spectra are offset for clarity.

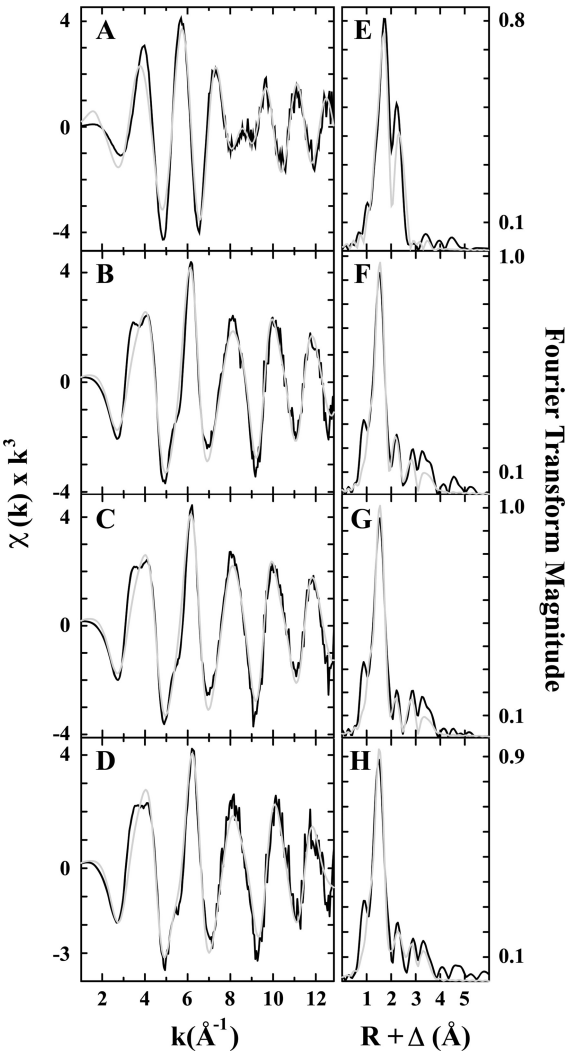

Figure 4. Copper EXAFS fitting analysis for *Methylocystis* sp. strain M pMMO. Raw EXAFS data for (A) reduced, (B) as-isolated, (C) Cu-reconstituted, membrane-bound, and (D) oxidized pMMO are shown in black. The reduced, as-isolated, and oxidized samples were solubilized. The phase shifted Fourier transforms of the copper data for (E) reduced, (F) as-isolated, (G) Cu-reconstituted, membrane-bound, and (H) oxidized are shown in black. Best-fit simulations are shown in gray.

In addition, long-range ligand interactions (>3 Å) are evident in all the spectra. EXAFS simulations show a mixture of Cu−O/N and Cu−Cu ligand environments in each of the samples, and an additional Cu−O/N environment was justifiably included for the reduced sample. Best-fit simulations to the average nearest-neighbor ligand environment included only Cu−O/N ligands with bond distances gradually decreasing from 2.02 Å (reduced pMMO) to 1.97 Å (as-isolated and Cu-reconstituted pMMO) to 1.96 Å (oxidized pMMO) (Tables 2, Tables S1−S4). The additional nearest-neighbor Cu−O/N environment in the reduced pMMO sample is at 2.15 Å. There is no evidence for Cu−S scattering. There was a significant improvement in all fits when a Cu−Cu scattering environment at >2.5 Å was included (Tables S1−S4). The Cu−Cu bond length of 2.64 Å for reduced pMMO is substantially longer than the 2.53 and 2.52 Å bond lengths observed for as-isolated or oxidized pMMO and Cu-reconstituted pMMO, respectively. The 2.64 Å Cu−Cu interaction in the reduced sample is different from the

Table 2. Summary of Cu EXAFS Fitting Analysis for *Methylocystis* sp. strain M pMMO[a]

	nearest-neighbor ligand environment[b]								nearest-neighbor ligand environment[b]				
sample	atom[c]	R (Å)[d]	CN[e]	σ^{2}[f]	atom[c]	R (Å)[d]	CN[e]	σ^{2}[f]	atom[c]	R (Å)[d]	CN[e]	σ^{2}[f]	F[g]
reduced	O/N	2.02	1	0.8	O/N	2.15	3	1.1	C	4.01	0.25	4.1	0.24
					Cu	2.64	0.75	4.3					
as-isolated	O/N	1.97	3	4.6	Cu	2.53	0.25	5.0	C	2.99	0.75	3.4	0.21
									C	3.30	1	5.9	
									C	3.90	2	4.9	
Cu-reconstituted	O/N	1.97	3	4.3	Cu	2.52	0.25	6.0	C	2.97	0.75	5.5	0.20
									C	3.30	1	3.6	
									C	3.89	2	5.4	
oxidized	O/N	1.96	3	5.1	Cu	2.53	0.25	3.7	C	2.85	0.75	5.6	0.25
									C	3.29	1	5.4	
									C	3.86	2	5.0	

[a]Data were fit over a k range of 1−12.85 Å^{-1}. [b]Independent metal−ligand scattering environment. [c]Scattering atoms: O (oxygen), N (nitrogen), and C (carbon), and Cu (copper). [d]Average metal−ligand bond length from three independent samples. [e]Average metal−ligand coordination number from three independent samples. [f]Average Debye−Waller factor in Å^2 × 10^3 from three independent samples. [g]Number of degrees of freedom weighted mean-square deviation between data and fit.

2.58 Å interatomic distance expected for Cu metal, suggesting that the integrity of the dinuclear metal center is maintained upon reduction. The occupancy for the Cu−Cu vector in the reduced sample is dramatically larger than the other three samples (CN of 0.75 vs 0.25, 0.25, and 0.25), suggesting that the Cu−Cu environment in all samples except the reduced may be heterogeneous with slightly different Cu−Cu vectors. In all samples, we were able to fit the data with long-range C scattering using single-scattering models. We were not able to fit long-range (>3 Å) scattering with a Cu−Cu interaction, also eliminating the possibility that our sample contains any appreciable Cu metal. Although fingerprints of Cu−imidazole scattering are apparent in the EXAFS of all samples (camelback beat pattern between k = 3−4 Å^{-1} and the shoulder at k = 5.5 Å^{-1}), attempts to fit any of the Cu EXAFS with a multiple scattering Cu−imidazole model were unsuccessful. Long-range Cu···C/N scattering, certainly resulting from the coordinated histidine residues, could, however, be adequately fit to the as-isolated, Cu-reconstituted, and oxidized samples EXAFS with single scattering models at bond lengths between 2.85 and 3.0 Å, at ca. 3.3 and 3.9 Å, bond lengths consistent with imidazoles. Overall, these results are consistent with data obtained for pMMO samples from *M. capsulatus* (Bath)[9] and *M. trichosporium* OB3b.[8]

Crystal Structure. The crystal structure of pMMO from *Methylocystis* sp. strain M was solved to 2.68 Å resolution (Table 3). Like pMMO from *M. capsulatus* (Bath) and *M. trichosporium* OB3b, *Methylocystis* sp. strain M pMMO is a trimer. Notably, strong density corresponding to a helix was observed adjacent to two of the three pmoC subunits and was modeled as polyalanine (Figure 5A). An unidentified helix is present at the same location in the 3.9 Å resolution *M. trichosporium* OB3b pMMO structure.[8] Although some side-chain electron density is apparent, it was not possible to determine the sequence of this helix.

The *Methylocystis* sp. strain M pmoB subunit is similar to the *M. capsulatus* (Bath) pmoB subunit with a root-mean-square deviation of 0.972 Å. The most pronounced differences are at the C-terminus, starting with an insertion in the *Methylocystis* sp. strain M pmoB sequence spanning residues 272−283. This region forms an extra loop structure, and as a result, the β strands encompassing residues 283−291, 302−308, and 358−364 are offset from the corresponding strands in the *M.*

Table 3. Data Collection and Refinement Statistics

	native (Cu anomalous)	Zn anomalous
data collection		
wavelength (Å)	1.37765	1.27816
resolution (Å)[a]	50−2.68 (2.75−2.68)	50−3.6 (3.66−3.60)
R_{sym}	0.146 (0.549)	0.201 (0.571)
$I/\sigma I$	19.2 (1.6)	20.1 (5.3)
completeness (%)	88.9 (54.4)	99.2 (94.3)
redundancy	12.6 (6.8)	12.3 (9.4)
refinement		
no. of reflections	83 726	
R_{work}/R_{free}[b]	0.249/0.281	
B-factor (Å2)	49.7	
rms deviations		
bond lengths (Å)	0.016	
bond angles (deg)	1.735	

[a]Values in parentheses refer to the highest-resolution shell. [b]For calculation of R_{free}, 5% of the reflections were reserved.

capsulatus (Bath) pmoB structure. The electron density for the pmoA subunit revealed a discrepancy with the model for *M. capsulatus* (Bath) pmoA. At residue Thr 196 (Thr 191 in *M. capsulatus* (Bath) pmoB), the electron density clearly extends along the periplasmic side of the membrane interface rather than leading through the membrane as in *M. capsulatus* (Bath) pmoA (Figure 5B). This extended loop region connects to a transmembrane helix spanning residues 217−244 and terminating at residue 252 on the cytoplasmic side of membrane. In *M. capsulatus* (Bath) pmoA, the region starting at Thr 191 is modeled as spanning the membrane to the cytoplasmic side and the helical region corresponding to *Methylocystis* sp. strain M residues 217−244 is modeled in the opposite direction (Figure 5B).

After tracing pmoA according to this new model, it became clear that the residues modeled as pmoA 195−215 in *M. capsulatus* (Bath) pMMO (Figure 5B) are actually part of pmoC and were therefore modeled as residues 178−197 of *Methylocystis* sp. strain M pmoC (Figure 5C). Finally, the C-terminal region of pmoC was traced with residues 225−252 extending from the periplasmic to cytoplasmic side, as opposed to residues 231−259 extending from the cytoplasmic to

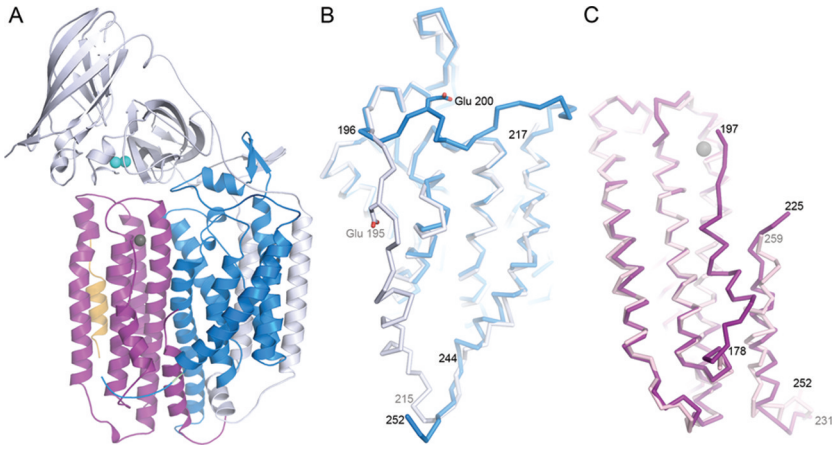

Figure 5. Structures of *Methylocystis* sp. strain M pMMO subunits. (A) One of the three protomers in the trimer. The pmoB, pmoA, and pmoC subunits are shown in gray, blue, and purple, respectively. Copper ions are shown in cyan, and a zinc ion is shown in gray. The additional helix is shown in yellow. (B) Superposition of the pmoA subunits from the *Methylocystis* sp. strain M (blue) and the original *M. capsulatus* (Bath) (gray) structures. (C) Superposition of the pmoC subunits from the *Methylocystis* sp. strain M (purple) and the original *M. capsulatus* (Bath) (light pink) structures. Residues discussed in the text are labeled.

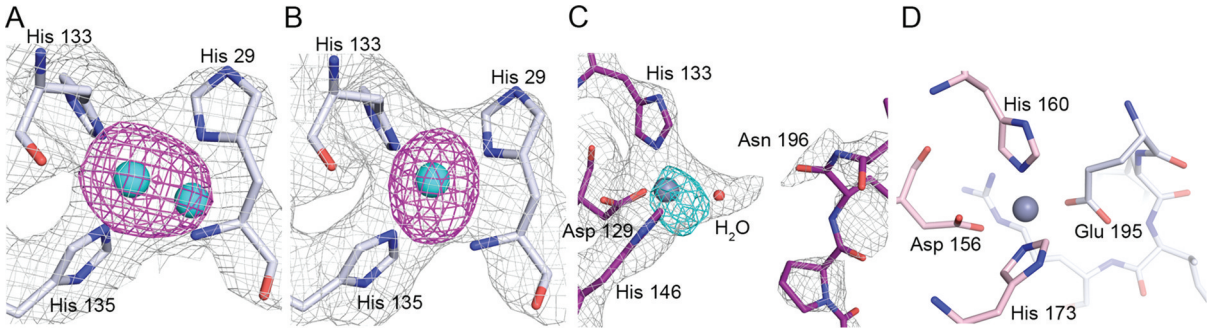

Figure 6. Metal centers in *Methylocystis* sp. strain M pMMO. The copper sites in (A) and (B) were modeled as dinuclear and mononuclear, respectively. The Cu anomalous map (magenta, 5σ) is superposed on the $2F_o - F_c$ map (1.4σ). (C) The zinc site is solvent exposed. The Zn anomalous map (cyan, 4.5σ) is superposed on the $2F_o - F_c$ map (1.4σ). (D) The zinc site as modeled in the original *M. capsulatus* (Bath) pMMO structure. The pmoC and pmoA subunits are colored light pink and gray as in Figure 5.

periplasmic side in the *M. capsulatus* (Bath) pmoC model. The orientation of this helix was also reversed in the *M. trichosporium* OB3b pMMO structure, but in that case, the low resolution precluded assigning any side chains.[8] The residues between 197 and 225 (Figure 5C) are not visible in the electron density map. The improved model for pmoC clearly indicates that it is not possible to connect the extra helix to this subunit and suggests that this helix derives from another yet to be identified polypeptide. Interestingly, this extra helix is not observed in the *M. capsulatus* (Bath) pMMO structure, suggesting its presence may be specific to pMMO from type II methanotrophs.

Examination of the electron density map for the original *M. capsulatus* (Bath) pMMO structure reveals poor density in the pmoA and pmoC regions that differ from those in the *Methylocystis* sp. strain M pMMO structure. Therefore, the *M. capsulatus* (Bath) pMMO structure was solved again by molecular replacement using the *Methylocystis* sp. strain M pMMO structure as a starting model. Following several refinement cycles, the final values of R_{work} and R_{free} were 0.269 and 0.296, respectively, as compared to 0.270 and 0.302 for the original structure.[6] Analysis with MolProbity[41] indicates that the new model is much better quality than the original model, with a Molprobity score of 3.20, corresponding to the 49th percentile of 4482 structures in the 2.80 ± 0.25 Å resolution range. The original model has a score of 3.85, corresponding to the 12th percentile. For comparison, the *Methylocystis* sp. strain M pMMO structure has a score of 2.93, corresponding to the 60th percentile of 5385 structures at 2.68 ± 0.25 Å resolution.

Anomalous Fourier maps of *Methylocystis* sp. strain M pMMO calculated using data collected at the Cu absorption edge (Table 3) exhibit strong (>15σ) peaks at the proposed dicopper active site. There are no peaks elsewhere in the structure, including within the C-terminal domain of pmoB, which is proposed by Chan and co-workers to bind 10 copper ions.[15] A dicopper site could be modeled in one of three pmoB subunits whereas the other two were best modeled with a single copper ion (Figure 6A,B). It is possible that the buffer exchange procedure involving multiple concentration and dilution steps removes some copper, which is consistent with the increased lability of copper binding to both *Methylocystis* sp. strain M and *M. trichosporium* OB3b pMMO.[8] The EXAFS data (Figure 4 and Table 2) indicate the presence of a short Cu−Cu interaction, supporting the modeling of a dicopper center in one of the pmoB subunits. A monocopper center corresponding to that in the *M. capsulatus* (Bath) pMMO structure[6] is not present, consistent with the substitution of an asparagine (Asn 44) for one of the histidine ligands. This monocopper site is

dx.doi.org/10.1021/bi200801z | *Biochemistry* 2011, 50, 10231−10240

not observed in the *M. trichosporium* OB3b pMMO structure either.[8]

Like *M. capsulatus* (Bath) pMMO, *Methylocystis* sp. strain M pMMO could be crystallized only in the presence of zinc. In addition to zinc ions mediating crystal contacts, the intramembrane site occupied by zinc in the *M. capsulatus* (Bath) pMMO structure is also occupied by zinc (Figure 6C,D). In the original *M. capsulatus* (Bath) pMMO structure, the zinc ion is coordinated by Asp 156, His 160, and His 173 from pmoC and Glu 195 from pmoA (Figure 6D). The new model for the pmoA and pmoC subunits drastically changes the environment at this site. While *Methylocystis* sp. strain M pmoC residues Asp 129, His 133, and His 146 are coordinated, Glu 200 from pmoA, which corresponds to Glu 195 in *M. capsulatus* (Bath) pMMO, points toward the N-terminal cupredoxin domain of pmoB (Figure 5B) and forms hydrogen bonds with the amide nitrogen atoms of pmoB residues Ser 109 and Gly 263. The fourth ligand to the zinc ion is instead modeled as a water molecule, which is within 4 Å of the carbonyl oxygen of Asn 196 (Figure 6C). The electron density is poor around Asn 196, and residues 197−225 could not be modeled. Therefore, it is also possible that the fourth coordination site is partially occupied by a disordered side chain from this region. As a result of the new model, the zinc site is exposed in the center of the pMMO trimer. The accessibility of this site is consistent with its occupation by zinc in the *Methylocystis* sp. strain M and *M. capsulatus* (Bath) pMMO structures and by copper in the *M. trichosporium* OB3b structure.[8] However, it seems less likely that a diiron active site could be accommodated in this position, as proposed by DiSpirito and co-workers.[12] Moreover, there is no evidence from anomalous data collected at the Fe absorption edge for iron binding sites in the *Methylocystis* sp. strain M pMMO structure. Finally, the hydrophilic patch of residues proposed to house a tricopper center[14] is devoid of metal ions in *Methylocystis* sp. strain M pMMO as it is in the *M. capsulatus* (Bath) and *M. trichosporium* OB3b structures.

In sum, pMMO from *Methylocystis* sp. strain M binds ∼2 copper ions per 100 kDa protomer and exhibits specific activity similar to that reported for *M. trichosporium* OB3b pMMO. As in the *M. trichosporium* OB3b and *M. capsulatus* (Bath) pMMOs, *Methylocystis* sp. strain M pMMO contains a mixture of Cu^{I} and Cu^{II} and exhibits type 2 Cu^{II} EPR signals. XAS data are also consistent with the presence of Cu^{I} and Cu^{II}. EXAFS data indicate the presence of a short Cu−Cu interaction, also observed in the other two pMMOs, and consistent with the dicopper active site model. The *Methylocystis* sp. strain M crystal structure, which is the best resolution and quality pMMO structure to date, provides revised models for the pmoA and pmoC subunits. These models led to an improved *M. capsulatus* (Bath) pMMO structure and a revised coordination environment for the crystallographic zinc/copper site. Taken together, these data are consistent with the dicopper active site model for pMMO.[11] The improvement of the pMMO structure is promising and suggests that a higher resolution view of the metal centers may be within grasp.

■ ASSOCIATED CONTENT

Supporting Information

Methods of EXAFS data analysis, tables summarizing progress of EXAFS simulations for all four samples, and EPR spectra of cyanide treated membrane-bound pMMO upon addition of copper. This material is available free of charge via the Internet at http://pubs.acs.org.

Accession Codes

The coordinates of *Methylocystis* species strain M pMMO and of *Methylococcus capsulatus* (Bath) pMMO have been deposited in the Protein Data Bank with accession codes 3RFR and 3RGB, respectively.

■ AUTHOR INFORMATION

Corresponding Author

*Tel 847-467-5301, Fax 847-467-6489, e-mail amyr@northwestern.edu (A.C.R.). Tel 313-577-5712, Fax 313-577-2765, e-mail tstemmle@med.wayne.edu (T.L.S.).

Present Address

[§]Department of Biological, Chemical and Physical Sciences, Roosevelt University, Chicago, IL 60605.

Funding

This work was supported by NIH grants GM70473 (A.C.R.), DK068139 (T.L.S.), and HL13531 (B.M.H).

■ ACKNOWLEDGMENTS

We thank Professor Hiroo Uchiyama for providing a culture of *Methylocystis* sp. strain M. Use of the Advanced Photon Source, an Office of Science User Facility operated for the U.S. Department of Energy (DOE) Office of Science by Argonne National Laboratory, was supported by the U.S. DOE under Contract DE-AC02-06CH11357. Use of the LS-CAT Sector 21 was supported by the Michigan Economic Development Corporation and the Michigan Technology Tri-Corridor (Grant 085P1000817). GM/CA CAT has been funded in whole or in part with Federal funds from the National Cancer Institute (Y1-CO-1020) and the National Institute of General Medical Science (Y1-GM-1104). XAS data were collected at SSRL, a national user facility operated by Stanford University on behalf of the U.S. Department of Energy, Office of Basic Energy Sciences. The SSRL Structural Molecular Biology Program is supported by the Department of Energy, Office of Biological and Environmental Research, and by the NIH, National Center for Research Resources, Biomedical Technology Program. We thank Sarah Sirajuddin for performing key crystallization screens and Dr. Rama Balasubramanian for valuable discussions and assistance with figure preparation.

■ ABBREVIATIONS

MMO, methane monooxygenase; sMMO, soluble MMO; pMMO, particulate MMO; EXAFS, extended X-ray absorption fine structure; EPR, electron paramagnetic resonance; XAS, X-ray absorption spectroscopy.

■ REFERENCES

(1) Hanson, R. S., and Hanson, T. E. (1996) Methanotrophic bacteria. *Microbiol. Rev. 60*, 439−471.

(2) Hakemian, A. S., and Rosenzweig, A. C. (2007) The biochemistry of methane oxidation. *Annu. Rev. Biochem. 76*, 223−241.

(3) Rosenzweig, A. C., Frederick, C. A., Lippard, S. J., and Nordlund, P. (1993) Crystal structure of a bacterial non-haem iron hydroxylase that catalyses the biological oxidation of methane. *Nature 366*, 537−543.

(4) Merkx, M., Kopp, D. A., Sazinsky, M. H., Blazyk, J. L., Müller, J., and Lippard, S. J. (2001) Dioxygen activation and methane hydroxylation by soluble methane monooxygenase: a tale of two irons and three proteins. *Angew. Chem., Int. Ed. 40*, 2782−2807.

(5) Tinberg, C. E., and Lippard, S. J. (2011) Dioxygen activation in soluble methane monooxygenase. *Acc. Chem. Res. 44*, 280−288.

(6) Lieberman, R. L., and Rosenzweig, A. C. (2005) Crystal structure of a membrane-bound metalloenzyme that catalyses the biological oxidation of methane. *Nature 434*, 177−182.
(7) Lieberman, R. L., and Rosenzweig, A. C. (2005) The quest for the particulate methane monooxygenase active site. *Dalton Trans. 21*, 3390−3396.
(8) Hakemian, A. S., Kondapalli, K. C., Telser, J., Hoffman, B. M., Stemmler, T. L., and Rosenzweig, A. C. (2008) The metal centers of particulate methane monooxygenase from *Methylosinus trichosporium* OB3b. *Biochemistry 47*, 6793−6801.
(9) Lieberman, R. L., Kondapalli, K. C., Shrestha, D. B., Hakemian, A. S., Smith, S. M., Telser, J., Kuzelka, J., Gupta, R., Borovik, A. S., Lippard, S. J., Hoffman, B. M., Rosenzweig, A. C., and Stemmler, T. L. (2006) Characterization of the particulate methane monooxygenase metal centers in multiple redox states by X-ray absorption spectroscopy. *Inorg. Chem. 45*, 8372−8381.
(10) Lieberman, R. L., Shrestha, D. B., Doan, P. E., Hoffman, B. M., Stemmler, T. L., and Rosenzweig, A. C. (2003) Purified particulate methane monooxygenase from *Methylococcus capsulatus* (Bath) is a dimer with both mononuclear copper and a copper-containing cluster. *Proc. Natl. Acad. Sci. U. S. A. 100*, 3820−3825.
(11) Balasubramanian, R., Smith, S. M., Rawat, S., Stemmler, T. L., and Rosenzweig, A. C. (2010) Oxidation of methane by a biological dicopper centre. *Nature 465*, 115−119.
(12) Martinho, M., Choi, D. W., DiSpirito, A. A., Antholine, W. E., Semrau, J. D., and Münck, E. (2007) Mössbauer studies of the membrane-associated methane monooxygenase from *Methylococcus capsulatus* Bath: evidence for a diiron center. *J. Am. Chem. Soc. 129*, 15783−15785.
(13) Semrau, J. D., DiSpirito, A. A., and Yoon, S. (2010) Methanotrophs and copper. *FEMS Microbiol. Lett. 34*, 496−531.
(14) Chan, S. I., Wang, V. C. C., Lai, J. C. H., Yu, S. S. F., Chen, P. P. Y., Chen, K. H. C., Chen, C. L., and Chan, M. K. (2007) Redox potentiometry studies of particulate methane monooxygenase: support for a trinuclear copper cluster active site. *Angew. Chem., Int. Ed. 46*, 1992−1994.
(15) Yu, S. S. F., Ji, C. Z., Wu, Y. P., Lee, T. L., Lai, C. H., Lin, S. C., Yang, Z. L., Wang, V. C. C., Chen, K. H. C., and Chan, S. I. (2007) The C-terminal aqueous-exposed domain of the 45 kDa subunit of the particulate methane monooxygenase in *Methylococcus capsulatus* (Bath) is a Cu(I) sponge. *Biochemistry 46*, 13762−13774.
(16) Lieberman, R. L., and Rosenzweig, A. C. (2004) Biological methane oxidation: regulation, biochemistry, and active site structure of particulate methane monooxygenase. *Crit. Rev. Biochem. Mol. Biol. 39*, 147−164.
(17) Basu, P., Katterle, B., Andersson, K. K., and Dalton, H. (2003) The membrane-associated form of methane monooxygenase from *Methylococcus capsulatus* (Bath) is a copper/iron protein. *Biochem. J. 369*, 417−427.
(18) Choi, D. W., Kunz, R. C., Boyd, E. S., Semrau, J. D., Antholine, W. E., Han, J. I., Zahn, J. A., Boyd, J. M., de la Mora, A. M., and DiSpirito, A. A. (2003) The membrane-associated methane monooxygenase pMMO and pMMO-NADH:quinone oxidoreductase complex from *Methylococcus capsulatus* Bath. *J. Bacteriol. 185*, 5755−5764.
(19) Nguyen, H. H., Elliott, S. J., Yip, J. H., and Chan, S. I. (1998) The particulate methane monooxygenase from *Methylococcus capsulatus* (Bath) is a novel copper-containing three-subunit enzyme. Isolation and characterization. *J. Biol. Chem. 273*, 7957−7966.
(20) Yu, S. S.-F., Chen, K. H.-C., Tseng, M. Y.-H., Wang, Y.-S., Tseng, C.-F., Chen, Y.-J., Huang, D. S., and Chan, S. I. (2003) Production of high-quality particulate methane monooxygenase in high yields from *Methylococcus capsulatus* (Bath) with a hollow-fiber membrane bioreactor. *J. Bacteriol. 185*, 5915−5924.
(21) Miyaji, A., Kamachi, T., and Okura, I. (2002) Improvement of the purification method for retaining the activity of the particulate methane monooxygenase from *Methylosinus trichosporium* OB3b. *Biotechnol. Lett. 24*, 1883−1887.
(22) Chan, S. I., and Yu, S. S. F. (2008) Controlled oxidation of hydrocarbons by the membrane-bound methane monooxygenase: The case for a tricopper cluster. *Acc. Chem. Res. 41*, 969−979.
(23) Smith, S. M., Balasubramanian, R., and Rosenzweig, A. C. (2011) Metal reconstitution of particulate methane monooxygenase and heterologous expression of the pmoB subunit. *Methods Enzymol. 495*, 195−210.
(24) Belford, R. L., and Belford, G. G. (1973) Eigenfield expansion technique for efficient computation of field-swept fixed-frequency spectra from relaxation master equations. *J. Chem. Phys. 59*, 853−854.
(25) Belford, R. L., and Nilges, M. J. (1979) Computer simulations of powder spectra, in EPR Symposium, 21st Rocky Mountain Conference, Denver, CO.
(26) George, G. N., George, S. J., and Pickering, I. J. (2001) EXAFSPAK, http://www-ssrl.slac.stanford.edu/~george/exafspak/exafs.htm.
(27) Ankudinov, A. L., and Rehr, J. J. (1997) Relativistic calculations of spin-dependent X-ray absorption spectra. *Phys. Rev. B 56*, R1712−R1715.
(28) Otwinowski, Z., and Minor, W. (1997) Processing of X-ray diffraction data collected in oscillation mode. *Methods Enzymol. 276*, 307−326.
(29) McCoy, A. J., Grosse-Kunstleve, R. W., Storoni, L. C., and Read, R. J. (2005) Likelihood-enhanced fast translation functions. *Acta Crystallogr. D61*, 458−464.
(30) Emsley, P., and Cowtan, K. (2004) Coot: model-building tools for molecular graphics. *Acta Crystallogr. D60*, 2126−2132.
(31) Murshudov, G. N., Vagin, A. A., and Dodson, E. J. (1997) Refinement of macromolecular structures by the maximum-likelihood method. *Acta Crystallogr. D53*, 240−255.
(32) Davis, I. W., Leaver-Fay, A., Chen, V. B., Block, J. N., Kapral, G. J., Wang, X., Murray, L. W., Arendall, W. B., Snoeyink, J., Richardson, J. S., and Richardson, D. C. (2007) MolProbity: all-atom contacts and structure validation for proteins and nucleic acids. *Nucleic Acids Res. 35*, W375−W383.
(33) Miyaji, A., Suzuki, M., Baba, T., Kamachi, T., and Okura, I. (2009) Hydrogen peroxide as an effecter on the inactivation of particulate methane monooxygenase under aerobic conditions. *J. Mol. Catal. B 57*, 211−215.
(34) Katterle, B., Gvozdev, R. I., Abudu, N., Ljones, T., and Andersson, K. K. (2002) A continuous-wave electron-nuclear double resonance (X-band) study of the Cu^{2+} sites of particulate methane mono-oxygenase of *Methylococcus capsulatus* (strain M) in membrane and pure dopamine beta-mono-oxygenase of the adrenal medulla. *Biochem. J. 363*, 677−686.
(35) Lemos, S. S., Collins, M. L. P., Eaton, S. S., Eaton, G. R., and Antholine, W. E. (2000) Comparison of EPR-visible Cu^{2+} sites in pMMO from *Methylococcus capsulatus* (Bath) and *Methlyomicrobium album* BG8. *Biophys. J. 79*, 1085−1094.
(36) Nguyen, H.-H. T., Nakagawa, K. H., Hedman, B., Elliott, S. J., Lidstrom, M. E., Hodgson, K. O., and Chan, S. I. (1996) X-ray absorption and EPR studies on the copper ions associated with the particulate methane monooxygenase from *Methylococcus capsulatus* (Bath). Cu(I) ions and their implications. *J. Am. Chem. Soc. 118*, 12766−12776.
(37) Chen, K. H.-C., Chen, C.-L., Tseng, C.-F., Yu, S. S.-F., Ke, S.-C., Lee, J.-F., Nguyen, H. T., Elliott, S. J., Alben, J. O., and Chan, S. I. (2004) The copper clusters in the particulate methane monooxygenase (pMMO) from *Methylococcus capsulatus* (Bath). *J. Chin. Chem. Soc. 51*, 1081−1098.
(38) Hung, S.-C., Chen, C.-L., Chen, K. H.-C., Yu, S. S.-F., and Chan, S. I. (2004) The catalytic copper clusters of the particulate methane monooxygenase from methanotropic bacteria: electron paramagnetic resonance spectral simulations. *J. Chin. Chem. Soc. 51*, 1229−1244.
(39) Balasubramanian, R., and Rosenzweig, A. C. (2007) Structural and mechanistic insights into methane oxidation by particulate methane monooxygenase. *Acc. Chem. Res. 40*, 573−580.
(40) Kau, L.-S., Spira-Solomon, D. J., Penner-Hahn, J. E., Hodgson, K. O., and Solomon, E. I. (1987) X-ray absorption edge determination

of the oxidation state and coordination number of copper. Application to the type 3 site in *Rhus vernicifera* laccase and its reaction with oxygen. *J. Am. Chem. Soc. 109*, 6433−6442.

(41) Chen, V. B., Arendall, W. B., Headd, J. J., Keedy, D. A., Immormino, R. M., Kapral, G. J., Murray, L. W., Richardson, J. S., and Richardson, D. C. (2010) MolProbity: all-atom structure validation for macromolecular crystallography. *Acta Crystallogr. D66*, 12−21.